CIRCADIAN RHYTHM

Circadian actin dynamics drive rhythmic fibroblast mobilization during wound healing

Nathaniel P. Hoyle,[1]* Estere Seinkmane,[1] Marrit Putker,[1] Kevin A. Feeney,[1] Toke P. Krogager,[1] Johanna E. Chesham,[1] Liam K. Bray,[1] Justyn M. Thomas,[2] Ken Dunn,[3] John Blaikley,[4] John S. O'Neill[1]*

Fibroblasts are primary cellular protagonists of wound healing. They also exhibit circadian timekeeping, which imparts an approximately 24-hour rhythm to their biological function. We interrogated the functional consequences of the cell-autonomous clockwork in fibroblasts using a proteome-wide screen for rhythmically expressed proteins. We observed temporal coordination of actin regulators that drives cell-intrinsic rhythms in actin dynamics. In consequence, the cellular clock modulates the efficiency of actin-dependent processes such as cell migration and adhesion, which ultimately affect the efficacy of wound healing. Accordingly, skin wounds incurred during a mouse's active phase exhibited increased fibroblast invasion in vivo and ex vivo, as well as in cultured fibroblasts and keratinocytes. Our experimental results correlate with the observation that the time of injury significantly affects healing after burns in humans, with daytime wounds healing ~60% faster than nighttime wounds. We suggest that circadian regulation of the cytoskeleton influences wound-healing efficacy from the cellular to the organismal scale.

INTRODUCTION

Circadian clocks allow organisms to organize behavior and physiology to an approximately 24-hour rhythm, facilitating adaptation to the environmental cycle of day and night. Although circadian rhythms in mammals are most evident at an organismal level, circadian timekeeping occurs cell-autonomously (1). The clock in every cell and tissue is synchronized in vivo by systemic cues such as body temperature and glucocorticoid signaling, which are themselves coordinated by a master clock in the hypothalamic suprachiasmatic nuclei (2). There is mounting evidence that circadian disruption, associated with modern lifestyles and aging, contributes to morbidities as diverse as cancer, cardiovascular disease, and diabetes (3, 4). A major knowledge gap exists, however, between the well-characterized circadian gene expression rhythms that occur in healthy peripheral tissues in vivo and the way in which different cell types exploit their innate clockwork to achieve beneficial circadian regulation of cell type–specific functions. The specific advantage conferred by the cell-intrinsic clockwork on cellular function has not been explored for most cell types but potentially holds the key to ameliorating the adverse effects of chronic circadian clock disruption.

The cellular clockwork is underpinned by cycles of "clock gene" expression, wherein complexes containing aryl hydrocarbon receptor nuclear translocator-like protein 1 (ARNTL/BMAL1) drive expression of E-box–regulated genes, including the transcriptional corepressor proteins period (PER) and cryptochrome (CRY), which eventually repress their own transcription. Beyond this core loop, BMAL1/PER/CRY-dependent expression of myriad "clock-controlled genes" facilitates differential control of cellular activity across each circadian cycle (5). In vivo, the core clockwork orchestrates a considerable proportion of the transcriptome (3 to 16%) to an approximately 24-hour program, with the identity of specific clock-controlled genes varying in a tissue-specific fashion (6).

Fibroblasts are a well-established model of the cell-autonomous clock and have robust circadian rhythms in clock gene expression (1). However, transcriptomic analyses of cultured fibroblasts have revealed very few circadian-regulated transcripts compared with the number observed in tissues from mice (>3000 in liver compared with 11 in fibroblast cultures) (7). This indicates that, in vivo, a considerable part of circadian transcriptional regulation is driven systemically (7). Proteomic analyses, which additionally incorporate posttranscriptional circadian regulation, have been applied to whole tissues from mice; however, the extent to which the cell-autonomous clock affects cellular protein abundance has not been investigated. The capacity of most cell types to keep time in isolation of systemic cues suggests functionality, but the advantage that it confers on fibroblast-specific cellular functions has not been interrogated (2).

Within the body, fibroblasts are mesenchymal cells that serve to secrete extracellular matrix, a function that is especially salient during wound healing. Upon wounding, fibroblasts respond to chemotactic cues that stimulate proliferation and migration into the affected area (8). Fibroblast motility is driven by actin polymerization at the leading edge of the cell to form protrusive lamellipodia and filopodia (9) and by disassembly of actin filaments at the trailing edge. Mutation of the actin-binding protein cyclase associated protein 2 (CAP2), for example, causes wound-healing defects in mice and reduced cell motility in scratch assays, associated with altered actin cytoskeletal dynamics and abnormal cell morphology (10).

Separately, it has been reported that certain parenchymal cell types exhibit circadian rhythms in actin polymerization, and this was suggested to be controlled by systemic circadian cues rather than the cell-autonomous clockwork (11). However, the putative driver of these actin rhythms has not been identified, and it is also not clear whether circadian regulation of the actin cytoskeleton has any functional consequence. One might anticipate that if circadian regulation of the actin cytoskeleton also occurs in mesenchymal cells, then this would confer an adaptive advantage on processes that are especially reliant on actin dynamics, such as cell motility during wound healing. It is established that clock gene mutant rodents exhibit impaired wound-healing phenotypes, but because clock genes have multiple functions beyond timekeeping, wound-healing defects cannot confidently be ascribed to

circadian dysfunction, and whether the actual capacity to heal shows a daily rhythm has not been investigated (*12–14*).

Here, we demonstrate that the cell-autonomous clock in fibroblasts drives a temporal proteomic program that imposes rhythmic regulation on the actin cytoskeleton. We explore the functional consequences of this rhythm and reveal that the cellular clock regulates wound healing in vitro, ex vivo, and in vivo through circadian control of cytoskeletal dynamics. Finally, we show that our findings are mirrored by a daily rhythm in the efficacy of healing in a post hoc analysis of human clinical burn data.

RESULTS

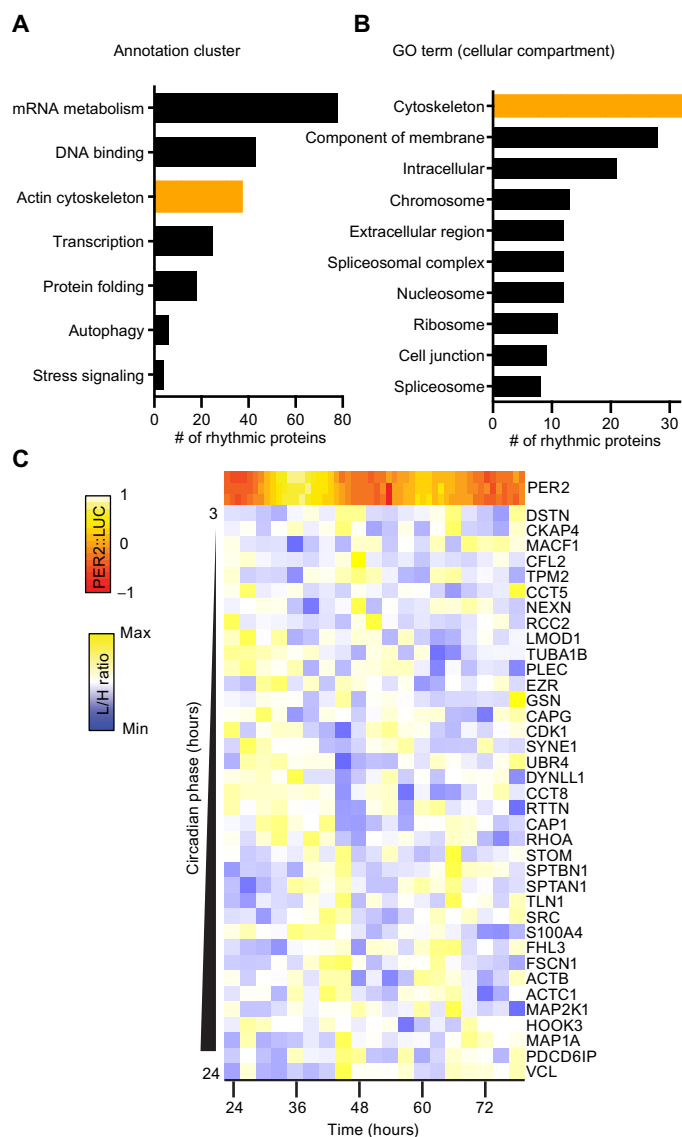### Defining the cell-intrinsic circadian proteome

Although previous studies have effectively shown the extent of cell-autonomous transcriptional rhythms, it has become increasingly apparent that posttranscriptional mechanisms contribute to determining how the cellular clockwork asserts control of biological function (*15–17*). Primary fibroblasts exhibit well-characterized circadian rhythms in clock gene activity, which persist under constant conditions for at least 6 weeks in vitro (*18*). To characterize the cell-autonomous circadian biology of fibroblasts, we performed a proteome-wide screen for proteins where abundance changes as a function of cellular circadian timing.

We quantified proteins in extracts from quiescent, confluent primary fibroblast cultures collected over two circadian cycles using SILAC (stable isotope labeling by amino acids in cell culture) followed by mass spectrometry. The primary fibroblasts were isolated and expanded from mice expressing PER2 fused with luciferase (PER2::LUC), which served as a parallel reporter of cellular timekeeping (*19*). Of 1608 proteins identified across the time course, 237 exhibited a robust circadian rhythm in abundance ($P < 0.010$; Fig. 1A and fig. S1) (*20*). Gene set enrichment analysis using the Database for Annotation, Visualization, and Integrated Discovery (DAVID) yielded several gene annotation clusters containing enriched terms (Fig. 1, A and B, and table S1) that related to mRNA metabolism, DNA binding, the actin cytoskeleton, transcription, protein folding, autophagy, and stress signaling (*21*).

Cellular processes associated with several of these clusters have been previously characterized as circadian, particularly transcription and DNA binding (*22*). Given the importance of the cytoskeleton in directing cell motility and thus fibroblast function, we were intrigued by the number of cytoskeletal regulators, specifically actin regulators such as cofilin 2 and Ras homolog family member A (RhoA), which were identified as rhythmic (Fig. 1C and fig. S2). Individual terms that make up the "actin cytoskeleton" cluster were not enriched ($P = 0.071$ to 0.168; table S1). This indicates that, although certain proteins show abundance rhythms, there is no wholesale regulation of the pathway. However, the number of rhythmic cytoskeletal regulators is highly suggestive that activity may be clock-regulated, given that rhythmic abundance of a single control node could be sufficient to render cytoskeletal activity circadian as a result.

### Cell-intrinsic clock control of actin dynamics

Actin dynamics exhibit circadian regulation in some peripheral tissues in vivo and are proposed to regulate clock gene expression in response to systemic cues (*11*). In light of our proteomics data, we asked whether actin dynamics might also be driven by the cell-intrinsic clockwork in the absence of systemic timing cues (Fig. 2A). To test this, actin polymeric state was assayed over two circadian cycles in confluent (quies-

Fig. 1. The cell-intrinsic fibroblast circadian proteome contains numerous cytoskeletal regulators. (**A**) Protein annotation clusters generated by DAVID containing terms enriched ($P < 0.10$) with rhythmic protein abundances identified by RAIN (Rhythmicity Analysis Incorporating Nonparametric methods) ($P < 0.01$) from the analysis of primary lung fibroblasts from PER2::LUC mice. (**B**) The 10 largest gene ontology (GO) (cellular compartment) terms within the rhythmic data set by protein number. (**C**) Mean abundance [light/heavy (L/H) ratio] of rhythmic proteins from the "actin cytoskeleton" cluster determined by three SILAC experiments with three parallel PER2::LUC measurements indicating the circadian phase (heat map).

cent) monolayers of PER2::LUC fibroblasts. We observed a circadian rhythm in F/G-actin ratio, with G-actin generally in excess of F-actin and without any consistent rhythm in total actin abundance (Fig. 2B).

Cytochalasin D (cytoD) (Fig. 2B) is a drug that binds both F- and G-actin, preventing their interaction with cofilin, thereby decreasing the rates of both actin polymerization and depolymerization (*23*). We found that the rhythm in F/G-actin ratio was disrupted by cytoD, indicating that fibroblast actin dynamics are normally under clock control. By phalloidin staining, we confirmed that cells treated with cytoD showed disruption of the actin cytoskeleton and noticed an increased
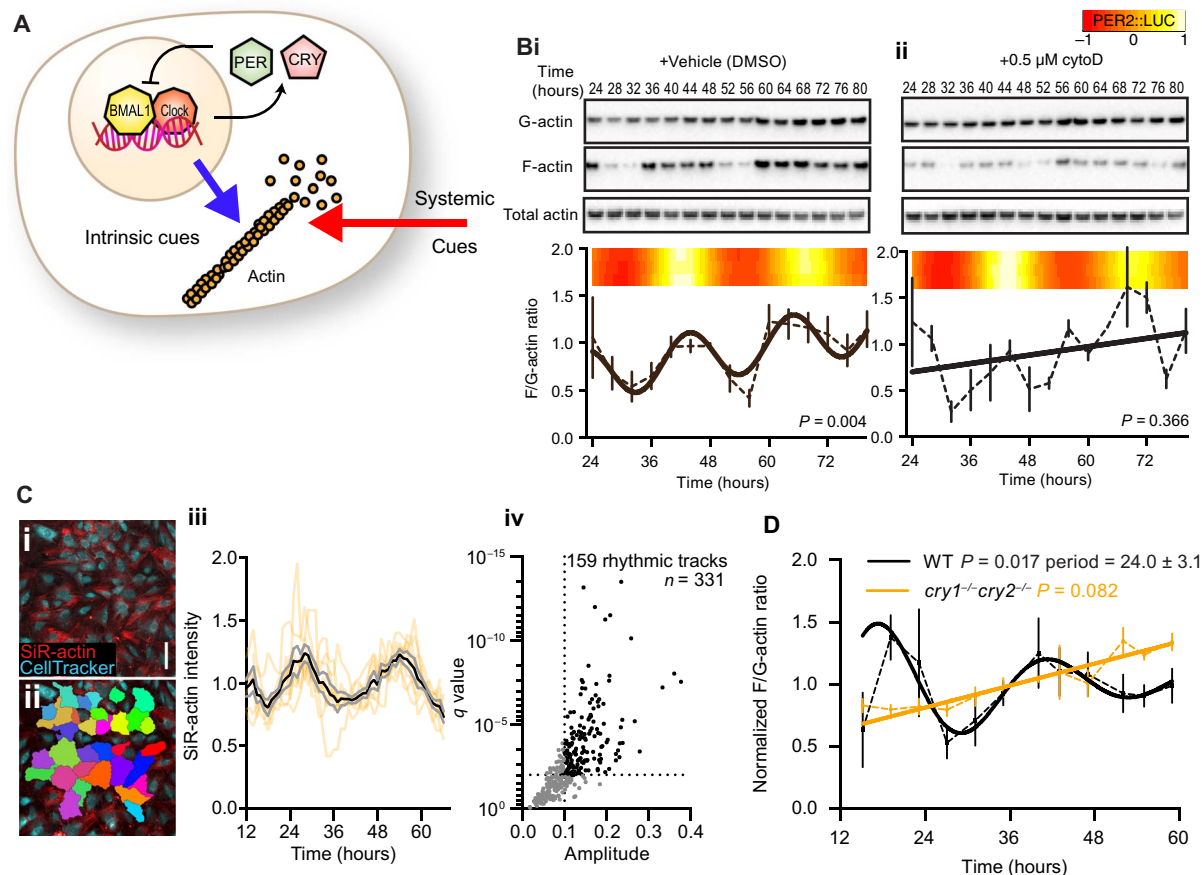
Fig. 2. CRY-dependent cell-intrinsic rhythms in actin polymerization. (**A**) Schematic depicting rhythms in actin polymerization, which may be cell-intrinsic (blue arrow; driven by circadian gene expression) in addition to systemic cues (red arrow). (**B**) Immunoblots using anti-actin antibody against fractionated and total protein from PER2::LUC fibroblasts at the indicated times after synchronization in the presence of dimethyl sulfoxide (DMSO) (i) or cytoD (0.5 μM) (ii). F/G-actin ratio is quantified below, with best-fit curves from a comparison of fits (n = 3; mean ± SEM). Three parallel bioluminescence measurements (heat map) are included as a marker for the circadian clock. Because G-actin was in excess, exposures between Western blot panels are not equivalent. (**C**) Live-cell recordings of actin abundance (SiR-actin) in cells labeled with CellTracker Green (i and ii; scale bar, 100 μm). (iii) SiR-actin intensity over time for eight individual tracks (orange lines) with mean (black) ± SEM (gray) overlaid. (iv) Tracks with a circadian harmonic regression FDR (q value) of <1% and amplitude of >10% of the mean are highlighted and quantified. (**D**) F/G-actin ratios from wild-type (WT; black line) or cry1−/− cry2−/− (orange line) fibroblasts at the indicated times after synchronization, with best-fit curves from a comparison of fits (n = 3; mean ± SEM); RAIN P values are indicated.

incidence of binuclearity, but no other major morphological defects were apparent. CytoD treatment had no effect on cellular circadian rhythms, as reported by PER2::LUC bioluminescence (Fig. 2B and fig. S3), and the fibroblast circadian clock was similarly resistant to other actin-modulating drugs (jasplakinolide and latrunculin A). This indicates that the circadian rhythms of actin dynamics do not strongly feed back into the cell-intrinsic circadian clock mechanism; rather, they are an output from it (fig. S3), and circadian bioluminescent reporter rhythms were therefore unaffected. The periods of the F/G-actin ratio rhythm and PER2:LUC were accordant, although the precise period of the F/G-actin rhythm could not be determined as accurately as the PER2::LUC continuous recording, due to the comparatively lower sampling frequency (every 4 hours versus every half hour) and its non-sinusoidal damping waveform.

Using the actin-binding silicon-rhodamine dye, SiR-actin (24), we validated the rhythm in the total abundance of F-actin in individual fibroblasts within a monolayer over 48 hours (Fig. 2C). Using harmonic regression analysis, we found that 48% of cells had significant rhythms

in F-actin [false discovery rate (FDR), <0.01 and amplitude, >10% mean) (25).

Transcriptionally arrhythmic CRY-deficient fibroblasts displayed no rhythm in F/G-actin ratio (Fig. 2D). Furthermore, we also observed F/G-actin rhythms in another fibroblast line (NIH3T3) derived from mouse embryonic tissue (fig. S4).

To summarize, using two independent methods, we detected cell-intrinsic circadian regulation of actin polymeric state that was dependent on cycling clock gene activity. We conclude that in fibroblasts, circadian regulation of actin dynamics is driven by cell-autonomous rhythms of clock gene expression.

A circadian rhythm in fibroblast wound healing

In vivo, the rapid fibroblast expansion at tissue wounds is known to result from both migration and proliferation of fibroblasts derived from local mesenchymal cells (8). To investigate the impact of actin cytoskeletal rhythms on cell migration, we performed wound-healing assays on synchronized monolayers of immortalized skin fibroblasts at

Hoyle et al., Sci. Transl. Med. **9**, eaal2774 (2017)   8 November 2017

3 of 10
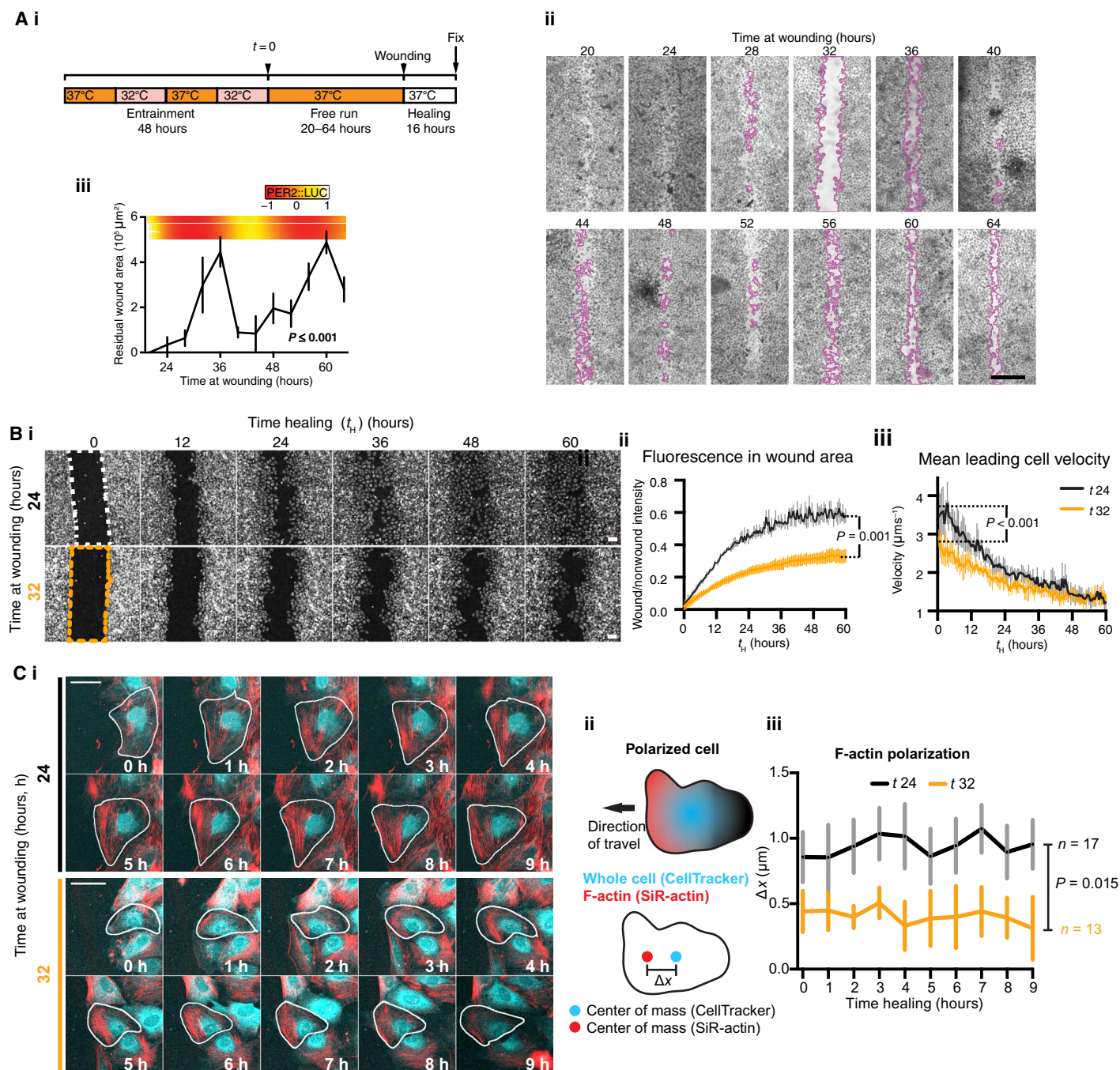
Fig. 3. A circadian rhythm in fibroblast wound-healing response. (**A**) (i) Fibroblast monolayers derived from adult PER2::LUC mouse skin were entrained and wounded after 20 to 64 hours in free run. (ii) Images of wound-healing assays; time at wounding is indicated, and residual wound is indicated by the highlighted area (pink) (scale bar, 500 μm). (iii) Quantification of the residual wound after 16 hours of wound healing (line) (n = 4; mean ± SEM) with three parallel PER2::LUC measurements (heat maps). RAIN P value is indicated. (**B**) (i) Fibroblasts labeled with CellTracker Red healing after wounding at the indicated times after synchronization (t). Scale bars, 100 μm. Wound healing (ii) and leading cell velocity (iii) are quantified (n = 4 or 5; mean ± SEM). P values from Tukey's multiple comparisons test after 60 hours of healing (t_H = 60) (ii) or t_H = 0 (iii) are indicated. (**C**) (i) Fibroblasts labeled with SiR-actin (red) and CellTracker Green (cyan) treated as in (B). Scale bars, 50 μm. A single cell for each condition has been highlighted in white with time healing indicated. The center of mass for each label (ii) was determined over 9 hours of healing, and the mean ± SEM degree of polarization (Δx) is indicated (iii). The P value from a two-way analysis of variance (ANOVA) is indicated.

different circadian phases over 2 days under constant conditions (Fig. 3A). The fibroblasts showed striking circadian variations in the residual wound area after 16 hours of healing, with minimal healing elicited by wounds inflicted just after the nadir of PER2 ex-

pression, at 32 to 36 hours and then at 56 to 60 hours after synchronization (Fig. 3A). In contrast, wounding at peak PER2 expression (20 to 24 or 44 to 48 hours after synchronization) was followed by efficient, near-complete healing of cell monolayers.

To monitor cell motility more closely, we followed fibroblast migration into wounds by confocal microscopy in cultures of fibroblasts at phases where we observed the maximal and minimal healing responses (24 and 32 hours after synchronization, respectively). Monolayers wounded after 24 hours reestablished more efficiently than those wounded after 32 hours, and this difference remained apparent after 60 hours of healing (Fig. 3B and movies S1 and S2). Cell division occurred infrequently in these cultures and had no circadian organization (fig. S5), suggesting that differential cell motility underpins the time-of-wounding effect. The initial velocity of the most motile 10% of cells was significantly greater for wounds inflicted 24 hours after synchronization compared with those wounded 32 hours after synchronization ($3.68 \pm 0.04 \, \mu m \, s^{-1}$ versus $2.78 \pm 0.03 \, \mu m \, s^{-1}$; $P < 0.0001$; Fig. 3B). There was no discernable circadian rhythm in cell velocity during healing, although circadian rhythms in PER2 expression remained evident throughout (fig. S6). Cell motility, cortical actin distribution, and cell size lacked any discernable circadian organization in the absence of wounding (fig. S6), indicating that the circadian variation in initial cell motility we observed is only unmasked on the insult of wounding. The circadian variation in F/G-actin and wound-healing response was absent in arrhythmic control fibroblasts lacking CRY proteins (fig. S7).

To assess how the circadian rhythm in actin dynamics might contribute to the time-of-wounding effect on healing, we used SiR-actin to dynamically follow actin distribution in cells undergoing healing. Wound-oriented polarization of F-actin in cells undergoing healing was consistently greater when monolayers were wounded 24 hours after synchronization rather than 32 hours after synchronization (Fig. 3C). This is indicative of more efficient F-actin enrichment at lamellipodia, the primary means by which fibroblasts affect migration (9). The time-dependent difference in F-actin polarization was sustained for at least the first 9 hours of healing. This is consistent with the migratory capacity of cells, adjacent to a nascent wound, being determined by the actin dynamical state at the circadian phase when the wound is incurred.

Uncoupling wound healing from the circadian clock

Cell adhesion is also dependent on the actin cytoskeleton. We thus thought that it is likely that BMAL1/PER/CRY-dependent circadian regulation of actin dynamics would also affect cell adhesion, which can be detected directly through measurement of cellular impedance (26). Accordingly, continuous recording of cellular impedance in PER2::LUC cultures revealed a CRY-dependent circadian oscillation, with greatest adhesion in phase with PER2 expression (Fig. 4A).

To establish causality, we reasoned that if PER/CRY-dependent oscillations in the abundance of actin regulators drive the rhythmic microfilament dynamics that underlie the rhythm in F/G-actin ratio, which in turn direct rhythmic adhesion and the time-of-wounding effect on migration, then cytoD disruption of the rhythm in actin dynamics (Fig. 2B) would attenuate both rhythmic outputs (27). To test this, we added 0.5 μM cytoD to PER2::LUC fibroblast monolayers and monitored impedance and the response to healing 24 or 32 hours after synchronization, as well as PER2 abundance in parallel. Compared with controls, we observed that cellular impedance rhythms were more severely damped and no longer showed a circadian rhythm in the presence of cytoD (Fig. 4A). Although cells still migrated after wounding in the presence of cytoD, they became insensitive to the time of wounding (Fig. 4B and fig. S8). Therefore, rhythmic wound healing and adhesion result from circadian control of actin dynamics but do not affect the cellular clock mechanism itself. Both circadian actin rhythms (Fig. 2)
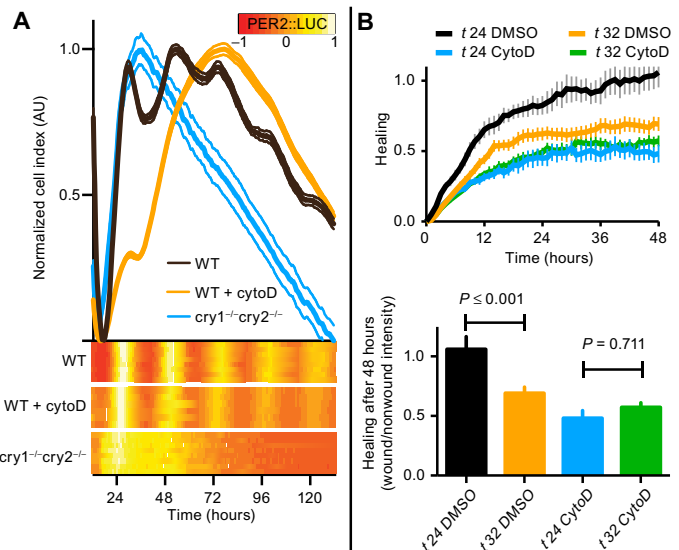
Fig. 4. Actin polymerization rhythms are required for circadian regulation of adhesion and wound-healing efficacy by fibroblasts. (**A**) Impedance measurements from $cry1^{-/-} \, cry2^{-/-}$ (blue) or wild-type fibroblasts treated with DMSO (black) or cytoD (orange) with simultaneous PER2::LUC measurements (heat maps) ($n = 6$ to 8; mean ± SEM). AU, arbitrary unit. (**B**) Quantification of mean fibroblast monolayer healing after wounding at the indicated times after synchronization (t) in the presence of 0.5 μM cytoD or vehicle ($n = 6$ to 12; mean ± SEM). P values from an ANOVA with Tukey's test for multiple comparisons are indicated.

and their consequences (Fig. 4) can be uncoupled from clock control by cytoD treatment, without affecting cellular timekeeping.

We considered that Rho activity might also contribute to the circadian differences in F/G-actin ratio, wound healing, and cell adhesion. Using the Rho inhibitor CT04, we observed damped rhythms in cell adhesion in PER2::LUC fibroblasts with only subtle effects on circadian rhythms in PER2 abundance (fig. S9). We performed wound-healing assays in cells treated with CT04 and observed abrogation of the time-of-wounding effect (fig. S9). The effect of Rho inhibition on impedance and wound-healing rhythms suggests that changes in Rho activity might also contribute toward transmitting circadian timing information to the cytoskeleton.

Diurnal fibroblast mobilization in vivo

To investigate the functional consequences of rhythmicity within the fibroblast actin cytoskeleton in the setting of an intact tissue, we measured fibroblast mobilization in an ex vivo murine skin explant model. Circadian rhythms in the skin of freely behaving mice have been demonstrated previously, and our in vitro experiments suggested that these would persist after wounding (28). Skin explants from PER2::LUC pups were mounted onto membranes, and bioluminescence was monitored to confirm that the peripheral circadian clock continues to function in cultured skin ex vivo (Fig. 5A). Subsequently, the skin from 5-day-old mouse pups was harvested in the middle of the resting period or early active phase, and the explant was wounded by biopsy punch and then mounted onto culture membranes. These times of day were chosen on the basis of our cell culture assays, being the times when we would expect to observe the greatest difference in cell migration. The migration of fibroblasts into heterologous blood clots filling the biopsy wounds was assayed by immunofluorescence staining against vimentin. We found that the number and total volume of fibroblasts invading
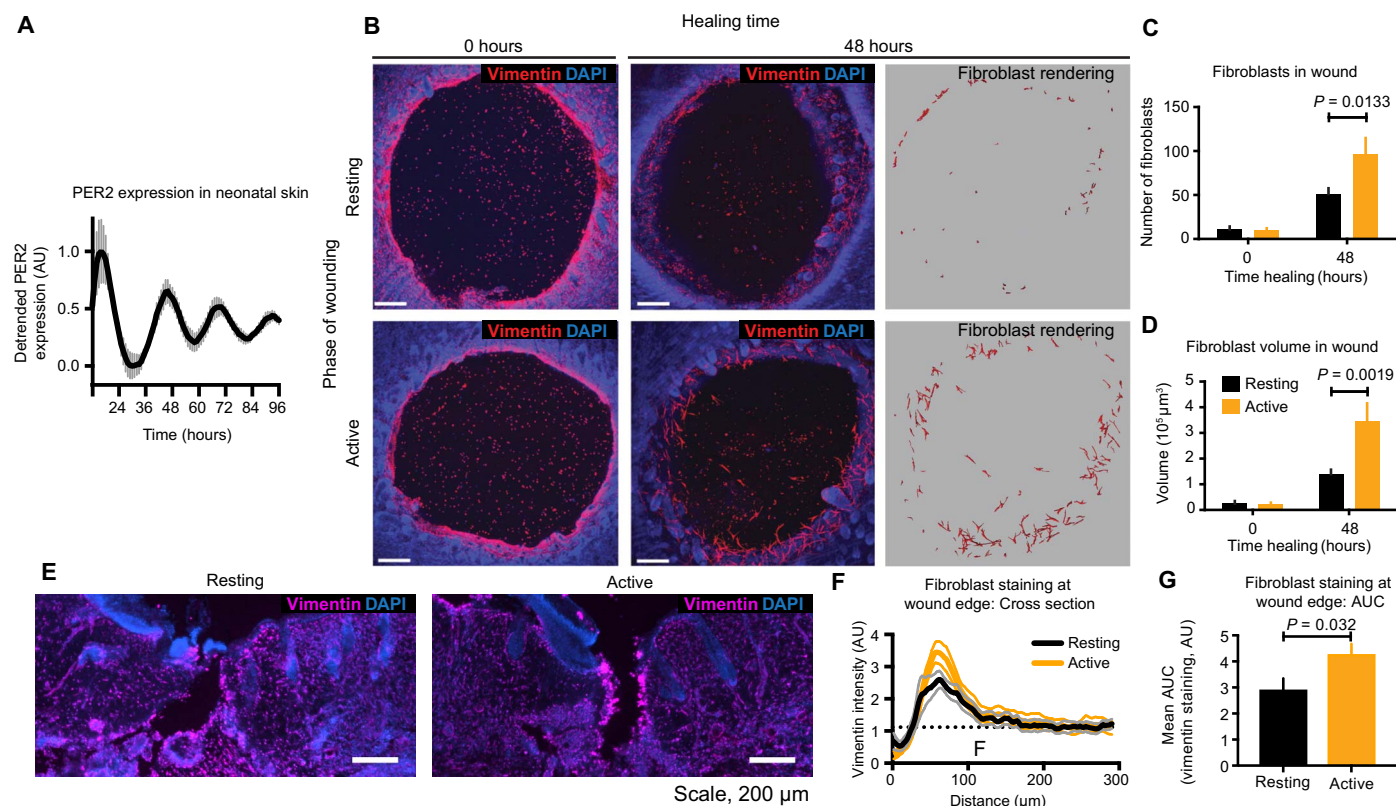
Fig. 5. Diurnal variation in wound-healing outcome and fibroblast mobilization. (**A**) Bioluminescence recording of PER2 expression in neonatal (P5) skin explants from PER2::LUC mice ($n = 6$; mean ± SEM). (**B**) Mouse skin wounds before and after 48 hours of healing. Fibroblasts were identified by anti-vimentin reactivity (red) and morphology and quantified by the number (**C**) and volume (**D**) ($n = 6$ to 7; mean ± SEM); Holm-Sidak's adjusted P value is indicated. Scale bars, 200 μm. DAPI, 4,6'-diamidino-2-phenylindole. (**E**) Transverse sections (60 μm) of mouse wounds made during the active and resting phases stained using anti-vimentin (magenta) and Hoechst (blue). (**F**) Cross-sectional vimentin staining across wound edges was quantified (mean ± SEM). (**G**) The area under the curve (AUC) was calculated using distal vimentin as a baseline [$n = 16$ (active) or 20 (resting); mean ± SEM]; The P value from a Student's t test is indicated.

the wound area were roughly twofold greater in skin explants collected during the active phase than those made during the resting period (Fig. 5, B to D, and movies S3 and S4). Finally, we wounded freely behaving adult mice by incision, again during the mid-resting or early active phases, and allowed them to heal for 48 hours (Fig. 5E). Fibroblast enrichment at the wound edge was again quantified using vimentin staining in transverse sections. Once more, we observed that fibroblast mobilization to wounds was significantly greater when wounds were inflicted during the active phase compared with the rest phase ($P < 0.032$; Fig. 5, F and G). This indicates that the degree of fibroblast mobilization in monolayers, skin explants, and mice is dependent on the time of wounding.

Within healing tissue, fibroblasts synthesize new extracellular matrix by deposition of collagen and fibronectin (29). Active-phase wounds might exhibit enhanced scar tissue formation due to increased collagen deposition, associated with more efficient fibroblast recruitment at this time. To test this, we inflicted bilateral wounds to the upper dorsal skin of mice by full-depth biopsy punch during the resting or active phase. We then allowed the skin to heal completely over 14 days before measuring collagen distribution around the healed volume. Epidermal collagen deposition was significantly increased above the sites of wounds that were incurred during the active phase compared with the rest phase ($P < 0.001$; fig. S10). In contrast to our observations at 2 days after wounding, fibroblasts no longer showed any significant

time-of-wounding difference after 14 days of healing (fig. S10). This is consistent with the expectation that fibroblasts numbers plateau at the wound site within 14 days (30).

Circadian rhythms in keratinocyte wound healing
Wound healing is a complex process involving multiple cell types in addition to fibroblasts. Keratinocytes migrate into nascent dermal wound areas, and any circadian modulation of this response would be expected to contribute to circadian regulation of wound healing in vivo (31). To test whether keratinocytes also display circadian wound-healing responses, we wounded synchronized monolayers of human keratinocyte (HaCaT) cells at times when fibroblast motility was at its peak or nadir, corresponding to the minimum or near-maximal *BMAL1* promoter activity, respectively (Fig. 6A). We observed a marked reduction in healing when cells were wounded at 32 hours after synchronization versus those wounded after 24 or 48 hours. There was no significant difference between the healing response when monolayers were wounded 24 or 48 hours after synchronization, consistent with keratinocyte migration also being regulated by the circadian clock (Fig. 6A).

A time-of-wounding effect in human burn injury outcome
The observation that migration of at least two major cell types involved in wound healing is circadian-regulated suggests that wound-healing
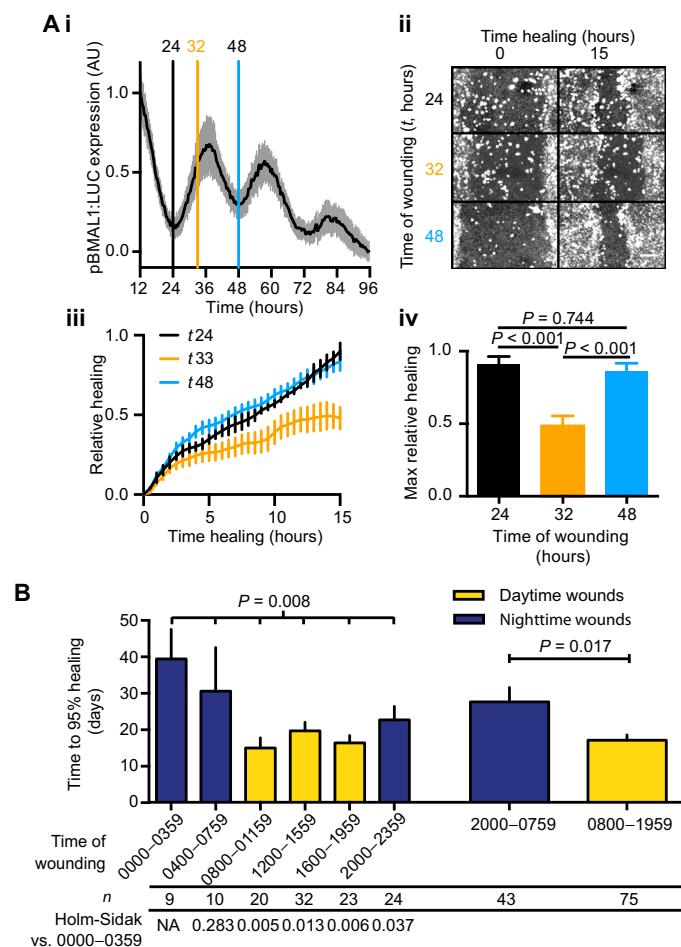
Fig. 6. A circadian rhythm in keratinocyte wound healing and a diurnal variation in human burn healing outcome. (**A**) (i) Synchronized HaCaT monolayers expressing luciferase under control of the BMAL1 promoter (n = 24; mean ± SD) were wounded at the indicated times (vertical lines), and (ii) healing was monitored by confocal microscopy. (iii) Relative fluorescence in the wound area (n = 4; mean ± SEM) was calculated, and (iv) maximal healing after 15 hours was compared by Tukey's multiple comparisons test (P values are indicated). (**B**) Mean time to 95% healing ± SEM from 118 human burn incidents separated by time of burn occurrence in 4-hour (left) or 12-hour (right) bins. ANOVA P value is indicated, as is the P value for Welch's t test comparing daytime versus nighttime wounds. P values from Holm-Sidak's test versus the 0000 to 0359 bin are indicated below. NA, not applicable.

efficiency, overall, might be influenced by the biological time of wounding. Although it is unknown whether wound healing is under circadian regulation in vivo, it has been reported that mice carrying mutations of circadian clock genes have impaired wound-healing phenotypes (*12*). If the circadian clock actively regulates tissue repair, timing the most effective healing to when wounds are more likely to occur, then we would expect to see time-of-day effects on wound healing. To this end, we analyzed historical clinical data from the international Burn Injury Database (iBID) and calculated the time required for human burn injuries to heal to 95% as a function of the time of day when the burn occurred (*32*). We observed an about 60% increase in healing time when burns occurred during the night compared with during the day (Fig. 6B). Although this post hoc analysis cannot prove that human wound healing is under clock control, we note that the time of day associated

with optimal healing for human burns patients is consistent with our results from rodent and cellular models: All occurred at biological times when mammals would be most active, when they are most likely to incur a wound (fig. S11).

DISCUSSION

Using a proteome-wide screen for rhythmic protein abundance, we identified a concerted regulation of 32 cytoskeletal proteins (GO:0005856). Mapping these onto the "Regulation of actin cytoskeleton" pathway (as defined by the Kyoto Encyclopedia of Genes and Genomes) revealed that several actin effector proteins, such as cofilin 2, and the key control node, RhoA, are rhythmically expressed (fig. S12). This concerted circadian regulation of the actin cytoskeleton generates rhythmic actin dynamics, which in turn modulate the ability of cells to respond appropriately at the moment of wounding—identifying a potentially important function of the cellular clock in a specific peripheral cell type. Our findings build on an earlier link between wound healing and the circadian clock identified by Kowalska *et al.* (*12*). Kowalska *et al.* used $per1^{-/-}/per2^{brdm/brdm}$ and $bmal1^{-/-}$ mutant mice, well-established genetic models that do not express circadian rhythms in behavior or gene expression. However, in addition to their molecular clock function, *PER1* and *PER2* are immediate-early genes and tumor suppressors, whereas *BMAL1* is a translation factor and regulator of the antioxidant response; consequently, some elements of each mutant's phenotype are now known to be unrelated to timekeeping function (*33–35*). Kowalska *et al.* reasonably focused on circadian gating of cell division as a basis for understanding circadian regulation of wound healing; we propose that circadian control of migration also plays a critical role. Using a combined in vitro and ex vivo approach, we demonstrate a circadian rhythm in the efficacy of wound healing, allowing us to rule out any substantial contribution of circadian gating of cell division to the differential ability of fibroblasts to enact wound healing in this context.

Our functional data show that circadian regulation of wound-evoked cell motility likely largely contributes to wound healing and epidermal collagen deposition in vivo in skin and other tissues. Cell-autonomous circadian regulation of migration was only unmasked in response to wounding, underpinned by clock gene–dependent temporal organization of actin dynamics, and associated with rhythmic cellular adhesion (fig. S11). That F-actin is conducive to efficient wound healing is explained by its role in protrusive force production at lamellipodia in migrating cells (*9*). Rho- and Rac-mediated signaling to the ARP2/3 complex, and resulting cytoskeletal changes modulate cell adhesion and migration (*36*). As expected, the adhesion rhythms we observed were attenuated by both cofilin and Rho inhibition, without disrupting clock gene expression cycles (Fig. 2 and fig. S9). Therefore, circadian regulation of the activity of cofilin, Rho, and other actin regulators is likely to be directly responsible for circadian actin dynamics in mammalian cells. Our findings complement reports of rhythmic Rho1 activity in the neurons of fruit flies and lead us to speculate that circadian regulation of the cytoskeleton may be a conserved phenomenon in metazoans (*37*). However, rather than circadian control of a single Rho activator, we observed distributed control of actin regulatory pathways (fig. S12), incorporating multiple regulators.

The observation that wound healing is more efficient during the active phase could inform future clinical practice and has clear translational potential. Unfortunately, we are currently unable to perform more in-depth analyses of the clinical data set, to rule out

Hoyle *et al.*, *Sci. Transl. Med.* **9**, eaal2774 (2017)   8 November 2017

7 of 10

severity changes over time for instance, due to the limitations of data collection and sample size. In the future, larger data sets should be gathered with circadian factors included. An experimental approach where wounds are produced in a controlled manner in a regulated environment would provide unequivocal evidence as to whether or not human wound healing is influenced by the circadian clock. We speculate that maximal healing could be promoted by pharmacological resetting of local cellular clocks before surgery, such as through topical application of chronoactive drugs (38).

Beyond adhesion and migration, the actin cytoskeleton is fundamental to eukaryotic cell biology, being essential to cell division, signal transduction, and pathogenesis (39–41). Its circadian regulation would therefore be likely to affect other aspects of biology of broad relevance to human health and disease.

MATERIALS AND METHODS

Study design
The primary objective was to investigate the role of circadian rhythms in controlling actin dynamics and fibroblast mobilization during wound healing. Data were generated by mass spectrometry and Western blotting on cell extracts, longitudinal bioluminescence assays, microscopic analysis of cultured cells, cellular electrical impedance assays, and immunofluorescence on fixed skin sections. For all experiments, replicate numbers are outlined in Materials and Methods or figure legends. Minimum sample size was determined by power analysis based on an estimated (from preliminary work) effect size with 15% σ and 5% type 1 error rate; replicates were included such that $1 - \beta = 0.9$. Mice in all experiments were age-matched and randomized into groups. Experimenters were not blinded to experimental groups, but where possible, automated analysis was used to remove bias. Adverse animal welfare issues were sufficient to halt experiments but did not arise during this work.

Cell culture and entrainment
Skin tissue from *Mus musculus* strain PER2::LUC was used to establish an immortalized fibroblast cell line as described previously (19, 42–44). $cry1^{-/-}$ $cry2^{-/-}$ fibroblast cells were similarly derived from otherwise isogenic $cry1^{-/-}$ $cry2^{-/-}$ mice (45). $cry1^{-/-}$ $cry2^{-/-}$ mouse embryonic fibroblasts (MEFs) and isogenic wild-type MEFs were obtained from A. Reddy. All mouse strains were gifts from M. Hastings and kept under the auspices of Home Office project license 70/7903, under UK Animals (Scientific Procedures) Act 1986. NIH3T3 fibroblasts and HaCaT cells stably expressing *pBMAL1*:LUC were made by transfecting cells [American Type Culture Collection (ATCC), CRL-1658; or HaCaT cells provided by A. Kramer (46)] with a construct encoding firefly luciferase downstream of the *BMAL1* promoter in pGL4.22 (Promega) and selected for puromycin resistance. Circadian entrainment was by 12-hour/12-hour 32°C/37°C temperature cycling for 3 days. For endpoint analysis, plates of cells were washed with phosphate-buffered saline and lysed at the specified time after the last entraining stimulus. Details of lysis and processing are included in Supplementary Materials and Methods. Circadian rhythmicity was assessed either by RAIN or by harmonic or nonlinear regression to a damped sine wave (see Supplementary Materials and Methods). Cells were maintained under conditions absolutely identical to the controls used for circadian bioluminescence recording in every case [see Supplementary Materials and Methods and Feeney *et al.* (47) for additional details].

Live cell actin analysis
Cells were labeled with 1 μM CellTracker Green (Thermo Fisher Scientific), and 100 nM SiR-actin (www.Cytoskeleton.org) was included in the medium throughout entrainment and image acquisition. A Leica SP8 confocal microscope with a 10×/0.40 objective was used to capture 7-μm z-sections covering the entire monolayer thickness every 60 min. Average z-projections were generated for each time point, and individual cells were tracked using the NIS-Elements General Analysis suite. The SiR-actin signal from each cell track over 24 hours long was subjected to harmonic regression analysis to determine rhythmicity (25).

For the analysis of F-actin distribution during healing, cells were delimited manually. The centers of mass for CellTracker Green (cell body) and SiR-actin (F-actin) were calculated using ImageJ (National Institutes of Health). The difference in position was calculated for each time point and used as a measure of the degree of actin polarization in the cell. We were not able to conduct a detailed analysis of stress fibers in these cultures due to limitations in spatial resolution and signal-to-noise ratio, both of which are essential to reliable identification of bona fide stress fibers.

Monolayer healing assays
Live-cell and endpoint scratch assays were performed by wounding synchronized monolayers at defined time points with a 200-μl plastic pipette tip and allowing healing at constant 37°C. Healing was assessed by the relative size of residual wound areas or using CellTracker dye–based assays on a confocal microscope, as detailed in Supplementary Materials and Methods.

Ex vivo wound-healing assays
PER2::LUC pups were raised in 12-hour light/dark (L/D) cycles from birth. For ex vivo assays, on P5, they were sacrificed by cervical dislocation at zeitgeber time (ZT) 5 or ZT13, where ZT0 is "lights on." Skin explants (~0.5 cm²) were obtained from each mouse, and 1.5-mm circular holes were made in the explants using a biopsy punch. The explants were then mounted onto 0.4-μm Millicell cell culture inserts (Millipore), and 4 μl of platelet-rich plasma + 10% calcium carbonate was added to each wound area and allowed to clot for 5 min. The explants were grown in Dulbecco's modified Eagle's medium + 10% HyClone III serum at 37°C and 5% CO_2 for 48 hours before fixation with 3% paraformaldehyde (PFA) and immunostaining for vimentin to identify fibroblasts.

In vivo wound healing
PER2::LUC mice were raised in 12-hour L/D cycles from birth. Age-matched (3- to 5-month-old) mice were shaved and wounded by a 1-cm incision at ZT5 or ZT13, where ZT0 is "lights on," and allowed to heal for 48 hours in 12-hour L/D cycles. Age-matched (1- to 2-month-old) mice were subjected to two bilateral full-thickness 1.5-mm circular biopsy punches to the upper back and allowed 14 days of healing in 12-hour L/D cycles. Mice were sacrificed, and wounded skin areas were excised and fixed with 4% PFA on 0.4-μm Millicell cell culture inserts (Millipore). Transverse sections (60 μm) were made in frozen gelatin before immunostaining. Fibroblasts were identified by immunostaining with rabbit anti-vimentin, mouse anti–platelet-derived growth factor receptor α (PDGFRα), or rabbit anti-CD26 antibody (Abcam) and Alexa Fluor 647–conjugated donkey anti-rabbit/mouse immunoglobulin G (Thermo Fisher Scientific). Fibroblast enrichment at the wound edge after 48 hours was measured as follows. The longest continuous wound edge from each section was manually traced. The mean

Hoyle *et al.*, *Sci. Transl. Med.* **9**, eaal2774 (2017)   8 November 2017

8 of 10

vimentin signal from the edge to 300 μm into the tissue was quantified along the length of the wound, giving vimentin signal versus distance from wound edge (Fig. 5F). The enrichment of vimentin was defined as the AUC, using the mean vimentin signal between 200 and 300 μM from the edge as the baseline (Fig. 5G). Fibroblast distribution after 14 days of healing was analyzed by mean fluorescence intensity from the apical edge of the signal at the center of the wound to a depth of 200 μm. Vimentin and PDGFRα stained the dermis, and CD26 stained the epidermis and dermis. The total signal for each fibroblast marker was quantified by AUC to a depth of 100 or 200 μm.

Collagen deposition was measured after 14 days by staining the sections for 3 hours with Col-F (ImmunoChemistry Technologies). The Col-F signal was quantified along the full thickness of the epidermis for >2 mm, centered on the wound. The Col-F was quantified by calculating the AUC using the distal signal as a baseline.

Human data

Anonymized records were obtained from a specialized iBID, which records outcomes from all the major burns units in England and Wales (32). In 2012, time of injury and number of days until 95% healing began to be recorded. Burns were included if a 95% heal time was recorded on the database and the subject had been admitted via the emergency department for their burn. Subject inclusion criteria were 18 to 60 years old with a body mass index between 20 and 30 kg/m^2. Subject records were excluded if they had any previous diseases or a skin graft was used in the treatment of their burn, leaving 118 patients in total (2012 to 2015).

Statistical analysis

For this study, we used the following statistical methods: GO enrichment analysis using DAVID, RAIN, the extra sum-of-squares F test for comparison of nonlinear regression fits, harmonic regression, two-way ANOVA with and without Tukey's multiple comparisons correction, two-way ANOVA with the Holm-Sidak adjustment, one-way ANOVA, Student's t test, and Welch's t test. They are each detailed along with the relevant parameters in Materials and Methods, Supplementary Materials and Methods, and figure legends. In general, a P value of <0.05 was considered significant, and a P value of <0.01 was considered highly significant. Individual subject-level data are shown in table S2.

SUPPLEMENTARY MATERIALS

www.sciencetranslationalmedicine.org/cgi/content/full/9/415/eaal2774/DC1
Materials and Methods
Fig. S1. Cell-intrinsic rhythms in the fibroblast proteome.
Fig. S2. Validation of cofilin 2 and RCC2 circadian abundance.
Fig. S3. Circadian clocks are robust against actin-modulating drugs.
Fig. S4. Cell-intrinsic rhythms in actin polymerization in NIH3T3 cells.
Fig. S5. Cell division in healing fibroblast monolayers.
Fig. S6. Cell area, velocity, and cortical actin distribution are not circadian in confluent cultures with circadian PER2::LUC activity.
Fig. S7. Circadian rhythms in actin dynamics and wound-healing efficacy are CRY-dependent in embryonic fibroblasts.
Fig. S8. Fibroblast monolayer healing in the presence of cytoD.
Fig. S9. Rho inhibition disrupts impedance rhythms and time-of-wounding effects without disrupting the circadian clock.
Fig. S10. Collagen deposition and fibroblast distribution after 14 days of healing.
Fig. S11. A model of clock control of wound healing.
Fig. S12. Circadian rhythmicity of the "Regulation of actin cytoskeleton" pathway.
Table S1. DAVID clustering of rhythmic proteins identified by RAIN ($P < 0.01$).
Table S2. Individual subject-level data for $n < 20$ (provided as an Excel file).

Movie S1. Healing of fibroblast monolayers wounded 24 hours after synchronization.
Movie S2. Healing of fibroblast monolayers wounded 32 hours after synchronization.
Movie S3. Fibroblast invasion of wounds made in the active phase after 48 hours of healing.
Movie S4. Fibroblast invasion of wounds made in the inactive phase after 48 hours of healing.
References (48–56)

REFERENCES AND NOTES

1. A. Balsalobre, F. Damiola, U. Schibler, A serum shock induces circadian gene expression in mammalian tissue culture cells. *Cell* **93**, 929–937 (1998).
2. U. Schibler, I. Gotic, C. Saini, P. Gos, T. Curie, Y. Emmenegger, F. Sinturel, P. Gosselin, A. Gerber, F. Fleury-Olela, G. Rando, M. Demarque, P. Franken, Clock-talk: Interactions between central and peripheral circadian oscillators in mammals. *Cold Spring Harb. Symp. Quant. Biol.* **80**, 223–232 (2015).
3. C. He, S. T. Anand, M. H. Ebell, J. E. Vena, S. W. Robb, Circadian disrupting exposures and breast cancer risk: A meta-analysis. *Int. Arch. Occup. Environ. Health* **88**, 533–547 (2015).
4. J. E. Gale, H. I. Cox, J. Qian, G. D. Block, C. S. Colwell, A. V. Matveyenko, Disruption of circadian rhythms accelerates development of diabetes through pancreatic beta-cell loss and dysfunction. *J. Biol. Rhythms* **26**, 423–433 (2011).
5. C. J. Doherty, S. A. Kay, Circadian control of global gene expression patterns. *Annu. Rev. Genet.* **44**, 419–444 (2010).
6. R. Zhang, N. F. Lahens, H. I. Ballance, M. E. Hughes, J. B. Hogenesch, A circadian gene expression atlas in mammals: Implications for biology and medicine. *Proc. Natl. Acad. Sci. U.S.A.* **111**, 16219–16224 (2014).
7. M. E. Hughes, L. DiTacchio, K. R. Hayes, C. Vollmers, S. Pulivarthy, J. E. Baggs, S. Panda, J. B. Hogenesch, Harmonics of circadian gene transcription in mammals. *PLOS Genet.* **5**, e1000442 (2009).
8. S. A. Eming, P. Martin, M. Tomic-Canic, Wound repair and regeneration: Mechanisms, signaling, and translation. *Sci. Transl. Med.* **6**, 265sr6 (2014).
9. M. Krause, A. Gautreau, Steering cell migration: Lamellipodium dynamics and the regulation of directional persistence. *Nat. Rev. Mol. Cell Biol.* **15**, 577–590 (2014).
10. K. Kosmas, A. Eskandarnaz, A. B. Khorsandi, A. Kumar, R. Ranjan, S. A. Eming, A. A. Noegel, V. S. Peche, CAP2 is a regulator of the actin cytoskeleton and its absence changes infiltration of inflammatory cells and contraction of wounds. *Eur. J. Cell Biol.* **94**, 32–45 (2015).
11. A. Gerber, C. Esnault, G. Aubert, R. Treisman, F. Pralong, U. Schibler, Blood-borne circadian signal stimulates daily oscillations in actin dynamics and SRF activity. *Cell* **152**, 492–503 (2013).
12. E. Kowalska, J. A. Ripperger, D. C. Hoegger, P. Bruegger, T. Buch, T. Birchler, A. Mueller, U. Albrecht, C. Contaldo, S. A. Brown, NONO couples the circadian clock to the cell cycle. *Proc. Natl. Acad. Sci. U.S.A.* **110**, 1592–1599 (2013).
13. L. Fu, H. Pelicano, J. Liu, P. Huang, C. Lee, The circadian gene *Period2* plays an important role in tumor suppression and DNA damage response in vivo. *Cell* **111**, 41–50 (2002).
14. R. V. Kondratov, A. A. Kondratova, V. Y. Gorbacheva, O. V. Vykhovanets, M. P. Antoch, Early aging and age-related pathologies in mice deficient in BMAL1, the core component of the circadian clock. *Genes Dev.* **20**, 1868–1873 (2006).
15. C. Jang, N. F. Lahens, J. B. Hogenesch, A. Sehgal, Ribosome profiling reveals an important role for translational control in circadian gene expression. *Genome Res.* **25**, 1836–1847 (2015).
16. M. S. Robles, J. Cox, M. Mann, In-vivo quantitative proteomics reveals a key contribution of post-transcriptional mechanisms to the circadian regulation of liver metabolism. *PLOS Genet.* **10**, e1004047 (2014).
17. F. Atger, C. Gobet, J. Marquis, E. Martin, J. Wang, B. Weger, G. Lefebvre, P. Descombes, F. Naef, F. Gachon, Circadian and feeding rhythms differentially affect rhythmic mRNA transcription and translation in mouse liver. *Proc. Natl. Acad. Sci. U.S.A.* **112**, E6579–E6588 (2015).
18. T. L. Leise, C. W. Wang, P. J. Gitis, D. K. Welsh, Persistent cell-autonomous circadian oscillations in fibroblasts revealed by six-week single-cell imaging of PER2:LUC bioluminescence. *PLOS ONE* **7**, e33334 (2012).
19. S.-H. Yoo, S. Yamazaki, P. L. Lowrey, K. Shimomura, C. H. Ko, E. D. Buhr, S. M. Siepka, H.-K. Hong, W. J. Oh, O. J. Yoo, M. Menaker, J. S. Takahashi, PERIOD2::LUCIFERASE real-time reporting of circadian dynamics reveals persistent circadian oscillations in mouse peripheral tissues. *Proc. Natl. Acad. Sci. U.S.A.* **101**, 5339–5346 (2004).
20. P. F. Thaben, P. O. Westermark, Detecting rhythms in time series with RAIN. *J. Biol. Rhythms* **29**, 391–400 (2014).
21. D. W. Huang, B. T. Sherman, Q. Tan, J. Kir, D. Liu, D. Bryant, Y. Guo, R. Stephens, M. W. Baseler, H. C. Lane, R. A. Lempicki, DAVID Bioinformatics Resources: Expanded annotation database and novel algorithms to better extract biology from large gene lists. *Nucleic Acids Res.* **35**, W169–W175 (2007).
22. N. Koike, S.-H. Yoo, H.-C. Huang, V. Kumar, C. Lee, T.-K. Kim, J. S. Takahashi, Transcriptional architecture and chromatin landscape of the core circadian clock in mammals. *Science* **338**, 349–354 (2012).

23. K. Shoji, K. Ohashi, K. Sampei, M. Oikawa, K. Mizuno, Cytochalasin D acts as an inhibitor of the actin–cofilin interaction. *Biochem. Biophys. Res. Commun.* **424**, 52–57 (2012).

24. G. Lukinavičius, L. Reymond, E. D'Este, A. Masharina, F. Göttfert, H. Ta, A. Güther, M. Fournier, S. Rizzo, H. Waldmann, C. Blaukopf, C. Sommer, D. W. Gerlich, H.-D. Arndt, S. W. Hell, K. Johnsson, Fluorogenic probes for live-cell imaging of the cytoskeleton. *Nat. Methods* **11**, 731–733 (2014).

25. S. Lück, K. Thurley, P. F. Thaben, P. O. Westermark, Rhythmic degradation explains and unifies circadian transcriptome and proteome data. *Cell Rep.* **9**, 741–751 (2014).

26. J. M. Atienza, J. Zhu, X. Wang, X. Xu, Y. Abassi, Dynamic monitoring of cell adhesion and spreading on microelectronic sensor arrays. *J. Biomol. Screen.* **10**, 795–805 (2005).

27. C. Hayot, O. Debeir, P. Van Ham, M. Van Damme, R. Kiss, C. Decaesteckter, Characterization of the activities of actin-affecting drugs on tumor cell migration. *Toxicol. Appl. Pharmacol.* **211**, 30–40 (2006).

28. T. Hamada, K. Sutherland, M. Ishikawa, N. Miyamoto, S. Honma, H. Shirato, K.-i. Honma, In vivo imaging of clock gene expression in multiple tissues of freely moving mice. *Nat. Commun.* **7**, 11705 (2016).

29. T. J. Shaw, P. Martin, Wound repair: A showcase for cell plasticity and migration. *Curr. Opin. Cell Biol.* **42**, 29–37 (2016).

30. I. Grierson, J. Joseph, M. Miller, J. E. Day, Wound repair: The fibroblast and the inhibition of scar formation. *Eye* **2** (Pt. 2), 135–148 (1988).

31. I. Pastar, O. Stojadinovic, N. C. Yin, H. Ramirez, A. G. Nusbaum, A. Sawaya, S. B. Patel, L. Khalid, R. R. Isseroff, M. Tomic-Canic, Epithelialization in wound healing: A comprehensive review. *Adv. Wound Care* **3**, 445–464 (2014).

32. N. Stylianou, I. Buchan, K. W. Dunn, A model of British in-hospital mortality among burns patients. *Burns* **40**, 1316–1321 (2014).

33. J. O. Lipton, E. D. Yuan, L. M. Boyle, D. Ebrahimi-Fakhari, E. Kwiatkowski, A. Nathan, T. Güttler, F. Davis, J. M. Asara, M. Sahin, The circadian protein BMAL1 regulates translation in response to S6K1-mediated phosphorylation. *Cell* **161**, 1138–1151 (2015).

34. E. S. Musiek, M. M. Lim, G. Yang, A. Q. Bauer, L. Qi, Y. Lee, J. H. Roh, X. Ortiz-Gonzalez, J. T. Dearborn, J. P. Culver, E. D. Herzog, J. B. Hogenesch, D. F. Wozniak, K. Dikranian, B. I. Giasson, D. R. Weaver, D. M. Holtzman, G. A. Fitzgerald, Circadian clock proteins regulate neuronal redox homeostasis and neurodegeneration. *J. Clin. Invest.* **123**, 5389–5400 (2013).

35. G. Yang, L. Chen, G. R. Grant, G. Paschos, W.-L. Song, E. S. Musiek, V. Lee, S. C. McLoughlin, T. Grosser, G. Cotsarelis, G. A. FitzGerald, Timing of expression of the core clock gene *Bmal1* influences its effects on aging and survival. *Sci. Transl. Med.* **8**, 324ra16 (2016).

36. J. E. Bear, J. M. Haugh, Directed migration of mesenchymal cells: Where signaling and the cytoskeleton meet. *Curr. Opin. Cell Biol.* **30**, 74–82 (2014).

37. A. Petsakou, T. P. Sapsis, J. Blau, Circadian rhythms in Rho1 activity regulate neuronal plasticity and network hierarchy. *Cell* **162**, 823–835 (2015).

38. M. Cuesta, N. Cermakian, D. B. Boivin, Glucocorticoids entrain molecular clock components in human peripheral cells. *FASEB J.* **29**, 1360–1370 (2015).

39. C. Esnault, A. Stewart, F. Gualdrini, P. East, S. Horswell, N. Matthews, R. Treisman, Rho-actin signaling to the MRTF coactivators dominates the immediate transcriptional response to serum in fibroblasts. *Genes Dev.* **28**, 943–958 (2014).

40. M. D. Welch, M. Way, Arp2/3-mediated actin-based motility: A tail of pathogen abuse. *Cell Host Microbe* **14**, 242–255 (2013).

41. Y.-W. Heng, C.-G. Koh, Actin cytoskeleton dynamics and the cell division cycle. *Int. J. Biochem. Cell Biol.* **42**, 1622–1633 (2010).

42. K. A. Feeney, L. L. Hansen, M. Putker, C. Olivares-Yañez, J. Day, L. J. Eades, L. F. Larrondo, N. P. Hoyle, J. S. O'Neill, G. van Ooijen, Daily magnesium fluxes regulate cellular timekeeping and energy balance. *Nature* **532**, 375–379 (2016).

43. M. Putker, P. Crosby, K. A. Feeney, N. P. Hoyle, A. S. H. Costa, E. Gaude, C. Frezza, J. S. O'Neill, Mammalian circadian period, but not phase and amplitude, is robust against redox and metabolic perturbations. *Antioxid. Redox Signal.*, 10.1089/ars.2016.6911 (2017).

44. A. Seluanov, A. Vaidya, V. Gorbunova, Establishing primary adult fibroblast cultures from rodents. *J. Vis. Exp.* **44**, e2033 (2010).

45. G. T. J. van der Horst, M. Muijtjens, K. Kobayashi, R. Takano, S.-i. Kanno, M. Takao, J. de Wit, A. Verkerk, A. P. M. Eker, D. van Leenen, R. Buijs, D. Bootsma, J. H. J. Hoeijmakers, A. Yasui, Mammalian Cry1 and Cry2 are essential for maintenance of circadian rhythms. *Nature* **398**, 627–630 (1999).

46. F. Spörl, K. Schellenberg, T. Blatt, H. Wenck, K.-P. Wittern, A. Schrader, A. Kramer, A circadian clock in HaCaT keratinocytes. *J. Invest. Dermatol.* **131**, 338–348 (2011).

47. K. A. Feeney, M. Putker, M. Brancaccio, J. S. O'Neill, In-depth characterization of firefly luciferase as a reporter of circadian gene expression in mammalian cells. *J. Biol. Rhythms* **31**, 540–550 (2016).

48. V. Baeker, N. Cahuzac, V. Georget, Montpellier RIO Imaging, ImageJ Macros; www.mri.cnrs.fr.

49. D. Franco, T. Franco, A. M. Schettino, J. M. T. Filho, F. S. Vendramin, Protocol for obtaining platelet-rich plasma (PRP), platelet-poor plasma (PPP), and thrombin for autologous use. *Aesthetic Plast. Surg.* **36**, 1254–1259 (2012).

50. B. M. Burkel, G. von Dassow, W. M. Bement, Versatile fluorescent probes for actin filaments based on the actin-binding domain of utrophin. *Cell Motil. Cytoskeleton* **64**, 822–832 (2007).

51. L. Bosgraaf, P. J. M. van Haastert, T. Bretschneider, Analysis of cell movement by simultaneous quantification of local membrane displacement and fluorescent intensities using Quimp2. *Cell Motil. Cytoskeleton* **66**, 156–165 (2009).

52. J. R. Wiśniewski, A. Zougman, N. Nagaraj, M. Mann, Universal sample preparation method for proteome analysis. *Nat. Methods* **6**, 359–362 (2009).

53. J. Cox, M. Mann, MaxQuant enables high peptide identification rates, individualized p.p. b.-range mass accuracies and proteome-wide protein quantification. *Nat. Biotechnol.* **26**, 1367–1372 (2008).

54. H. J. Motulsky, R. E. Brown, Detecting outliers when fitting data with nonlinear regression—A new method based on robust nonlinear regression and the false discovery rate. *BMC Bioinformatics* **7**, 123 (2006).

55. D. K. Welsh, S.-H. Yoo, A. C. Liu, J. S. Takahashi, S. A. Kay, Bioluminescence imaging of individual fibroblasts reveals persistent, independently phased circadian rhythms of clock gene expression. *Curr. Biol.* **14**, 2289–2295 (2004).

56. J. S. O'Neill, M. H. Hastings, Increased coherence of circadian rhythms in mature fibroblast cultures. *J. Biol. Rhythms* **23**, 483–488 (2008).

Citation: N. P. Hoyle, E. Seinkmane, M. Putker, K. A. Feeney, T. P. Krogager, J. E. Chesham, L. K. Bray, J. M. Thomas, K. Dunn, J. Blaikley, J. S. O'Neill, Circadian actin dynamics drive rhythmic fibroblast mobilization during wound healing. *Sci. Transl. Med.* **9**, eaal2774 (2017).

Science Translational Medicine

Circadian actin dynamics drive rhythmic fibroblast mobilization during wound healing

Nathaniel P. Hoyle, Estere Seinkmane, Marrit Putker, Kevin A. Feeney, Toke P. Krogager, Johanna E. Chesham, Liam K. Bray, Justyn M. Thomas, Ken Dunn, John Blaikley and John S. O'Neill

Time heals all wounds

Disrupting circadian rhythm, the 24-hour cycle corresponding to light and darkness, is associated with disease and aging. Here, Hoyle *et al.* discovered a role for circadian control in wound healing. Skin wounds in mice wounded during the circadian rest period healed less quickly than those wounded during the active period. The authors uncovered a circadian regulation of actin, a cytoskeletal protein involved in cell migration, in fibroblasts in the wound-healing response. Analysis of a database of human burn injuries showed that those incurred during the night (rest period) healed more slowly than wounds acquired during the day (active period). This work extends our understanding of cell-autonomous clock control.

ARTICLE TOOLS	http://stm.sciencemag.org/content/9/415/eaal2774
SUPPLEMENTARY MATERIALS	http://stm.sciencemag.org/content/suppl/2017/11/06/9.415.eaal2774.DC1
RELATED CONTENT	http://stm.sciencemag.org/content/scitransmed/7/305/305ra146.full http://stm.sciencemag.org/content/scitransmed/2/31/31ra33.full http://stm.sciencemag.org/content/scitransmed/4/129/129ra43.full http://stm.sciencemag.org/content/scitransmed/8/324/324ra16.full http://stm.sciencemag.org/content/scitransmed/6/265/265sr6.full
REFERENCES	This article cites 54 articles, 12 of which you can access for free http://stm.sciencemag.org/content/9/415/eaal2774#BIBL
PERMISSIONS	http://www.sciencemag.org/help/reprints-and-permissions

Use of this article is subject to the Terms of Service